ALFVÉN WAVE HEATING AND RUNAWAY DISCHARGES IN THE TCABR TOKAMAK

R.M.O. Galvão,V Bellintani Jr., A.G. Elfimov, J.I. Elizondo, A.N. Fagundes, A.A. Ferreira, A.M.M. Fonseca, Yu.K. Kuznetsov, E.A. Lerche, I.C. Nascimento, E.M. Ozono, L.F. Ruchko, W.P. de Sá, E.A.O. Saettone, E.K. Sanada, J.H.F. Severo, R.P. da Silva, V.S. Tsypin, O.C. Usuriaga, A. Vannucci

Institute of Physics, University of São Paulo, CEP 05315-970, São Paulo, Brazil

Recent results of experiments on Alfvén wave heating and runaway discharges carried out in the TCABR tokamak are presented. A new antenna type has been installed to allow wave excitation with higher RF currents and lower dynamic polarization of the antenna straps than for the one previously used. In spite of edge plasma heating, which causes influx of impurities, we have obtained a clear confirmation of wave deposition inside the plasma from a localized increase of the electron temperature measured with the ECE radiometer. Detailed profiles of the plasma density and H_α emission were obtained in runaway disharges with currents around 100 kA. These profiles confirm our model of a low-temperature plasma maintained in equilibrium by the relativistic electron beam. Analysis of the H_α and density spikes indicate that recombination plays a substantial role in the particle and energy balance.
PACS: 52.55.Fa; 52.35.Bj

1.INTRODUCTION

Alfvén wave heating and current drive is being intensively investigated in the TCABR tokamak (R_0 = 0.61m, a = 0.18m, B_ϕ = 1.1T, $I_P \le 120$kA, $n_0 \le 4\times10^{19}$ m^{-3}). Numerical codes in cylindrical and toroidal geometry were developed to analyze the mode structure excited inside the plasma and determine the best experimental conditions for efficient plasma heating and non-inductive current drive [1]. One antenna module with four poloidal loops was installed and both plasma heating and current drive in intermediate power regime have been achieved under different plasma conditions [2,3]. The experimental impedance curves show good agreement with theoretical predictions (including the narrow peaks expected for the Global Alfvén eigenmodes (GAW)). Nevertheless, the power input was limited to less than 100 kW, due to high antenna dynamic polarization and consequent strong interaction with the plasma periphery.

With the purpose of improving the efficiency in high power heating experiments, the original antenna system was modified to reduce the antenna self-inductance, ensure better lateral protection with BN plates, and alter the feeding configuration. A module of the new antenna has already been installed and the first experimental results are presented in this paper.

The new regime of runaway discharges found in TCABR was further investigated [4]. The radial profiles of plasma density and H_α emission were determined under different fluxes of neutral gas injection. Analysis of the spikes in H_α emission and loop voltage allows to estimate the temperature of the background plasma. The results confirm our early model of a cold plasma, dettached from the limiter, maintained in equilibrium by the relativistic runaway beam.

2. ANTENNA STRUCTURES

The Alfvén wave excitation system originally designed for TCABR consists of four antenna modules, equally spaced in the toroidal direction, with four poloidal loops in each module. The RF power is supplied by a four-phase oscillator capable of delivering up to 1MW in the f = 2-8 MHz range [2].

Before installing the four modules, we have decided to first test a single module with two different antenna structures, designated by type I and type II antennae. Both consist of two pairs of poloidal straps separated toroidally by aproximately 22°. For the former type, each strap is a full loop that is cut in two half-turn windings fed in parallel. The loops of each pair are rotated 90° in the poloidal direction with respect to each other, reducing the mutual coupling between them and allowing the excitation of single helicity traveling modes (M = +1 or M = -1) [2]. For type II antenna, the poloidal extension of the windings has been reduced to approximately 90° and the width has practically doubled, decreasing the self-inductance by a factor about three with respect to the type I. The straps of each pair are placed symmetrically in relation to the equator of the vacuum chamber, in the upper and lower external corners. In this case, both main poloidal modes (M = +1 and M = -1) may be simultaneously excited.

Results of numerical calculations of the vacuum field produced by one module of the antenna system indicate that while type I antenna provides a rather good poloidal mode selection, exciting only the main mode M = -1 and its first harmonic M = +3 with reduced amplitude, the second antenna excites the M = ±1 modes simultaneously, together with small components of all other low order poloidal harmonics.

The spectrum of waves actually excited in the plasma depends on a proper choice of the frequency and plasma conditions, mainly plasma density and current. Results of simulations carried out with a cylindrical code, based upon the fluid model developed by Appert et al. [5], show that, as expected, type I antenna produces a single poloidal wavenumber M = -1 spectrum, while with the second type, harmonics with M = ±1 (and even M = ±2) also exist. The toroidal spectra, with mainly N = -2, -1, +2 and small N = -3, +3 components, for $n_0 = 3\times10^{19}$ m^{-3}, are quite similar in both cases.

3. RESULTS OF ALFVÉN HEATING EXPERIMENTS

The measured coupling impedance Z_p is shown in Fig. 1, for the two antenna types, as function of the central line density.

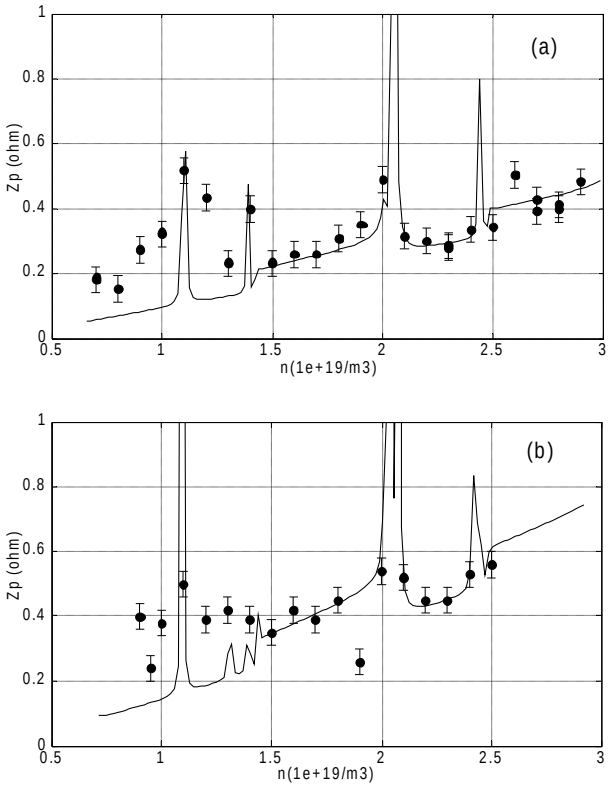

Fig. 1. Experimental values of the coupling impedance (Z_P) as function of line density for type I, f= 3.9 MHz (a), and type II, f = 4 MHz (b), antennae, fed with phasing (0,π). The continuous curves represent the impedance curve calculated with the cold cylindrical model.

For higher densities and thus more collisional plasmas, the impedance curve of the cold model fits the experimental data well, including the global resonance M = -1, N = -3 located near $\overline{n} \approx 2.0\times 10^{19}\, m^{-3}$. However, for densities less than $\overline{n} = 1.5\times 10^{19}\, m^{-3}$, the experimental values are significantly higher than expected. Also the resonance at $\overline{n} = 1.1\times 10^{19}\, m^{-3}$ seems to be broader then predicted by the cold cylindrical model. One possible explanation for this discrepancy is the contribution of side-band poloidal harmonics with M = 0 to the plasma impedance in this low-density region. These harmonics only appear when toroidal corrections are taken into account. Considering the impedances in vacuum, we see that the coupling efficiency in the continuum is approximately 30% and 50%, for antenna types I and II, respectively.

The effect of RF power deposition around the broad resonance at $\overline{n} \approx 1.1\times 10^{19}\, m^{-3}$ can be seen in Fig. 2 for discharge 7379. During the current plateau, the plasma density was kept approximately constant by using a high-speed programmable gas puffing system. The f =3.9 MHz and P = 80 kW RF pulse was switched on at t = 67 ms and lasted approximately 10 ms.

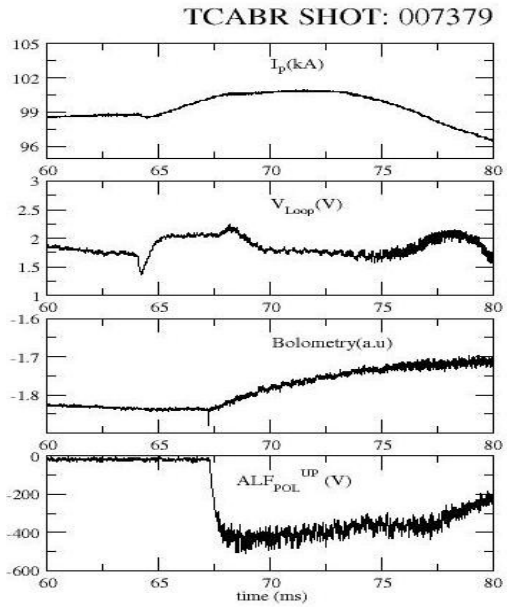

Figure 2. Plasma discharge 7379 with Alfvén wave heating using type I antenna: a) plasma current, b) loop voltage, c) bolometer signal d) dynamic polarization voltage of the antenna. The RF pulse starts at t=67 ms and lasts 10 ms.

The dynamic polarization of the antenna increases rapidly with the RF pulse, reaching a negative value close to 430 V in approximately 2 ms. This causes an increase of the impurity flow into the plasma, as can be seen by the increase in the radiated power detected by the bolometer. Nevertheless, an indication of plasma heating or current drive can be seen in the loop voltage and current traces. As can be seen in Fig. 2(b), the loop voltage increases slightly at the beginning of the RF pulse, in response to the impurity inflow. Approximately 1 ms later, it starts to drop while the current stays constant for a period around 5 ms [Fig. 2(a)]. The RF power starts to decrease at t ≈ 76 ms and the loop voltage increases while the plasma current drops, indicating plasma cooling or quenching of the RF driven current. The hump in the loop voltage signal at t = 64 ms is produced by the main inductive circuit to elongate the flat current region of the discharge.

The deleterious edge coupling is substantially reduced with type II antenna, due mainly to its lower inductive load. This can be seen in the time traces for discharge 8294, shown in Fig. 3. In this case, approximately 80 kW of RF power, f = 4 MHz, was applied to two loops of type II antenna, at t = 55 ms, with (0,π) phase. Under this phasing condition, a broad spectrum of waves can be excited, including standing waves close to the plasma boundary. Nevertheless, the dynamic polarization of the antenna decreases by a factor of approximately two, in comparison with type I antenna under similar plasma conditions [Fig. 2], the increase in radiated power is smaller, and there is no noticeable increase in the loop voltage.

It is interesting to note that, while the loop voltage keeps decreasing monotonically, the plasma current increases slightly during the RF pulse.

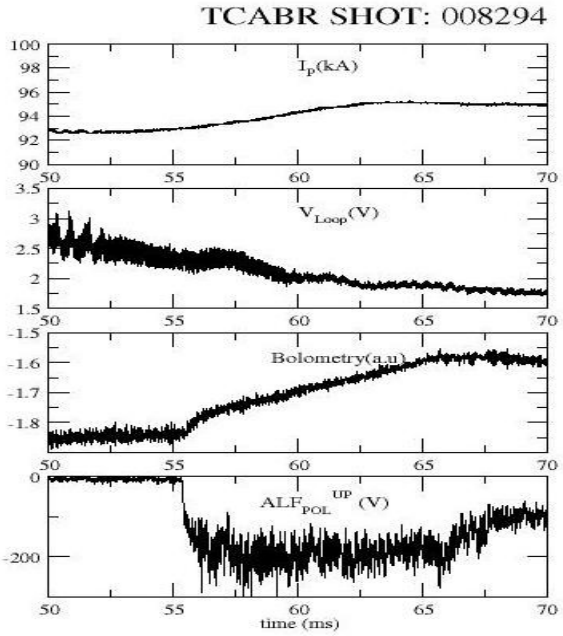

Fig. 3. Plasma discharge 8294 with Alfvén wave heating using type II antenna : a) plasma current, b) loop voltage, c) bolometer signal d) dynamic polarization voltage of the antenna. The RF pulse starts at t=55 ms and lasts 10 ms.

This can be interpreted as an indication of direct current drive or plasma heating. Fortunately, towards the end of this campaign, an ECE radiometer became available and the relative modification of the temperature profile during the RF pulse could be measured. The result for shot 8545 can be seen in Fig. 4, where the time traces of electron temperature in six radial positions of the plasma column are shown. The large peaks at the beginning are due to non-thermal emission during plasma formation and current ramp-up. The thermal emission starts approximately at 18 ms after breakdown. The temperature trace at the outmost radial position, R ≈ 0.73 m shows a somewhat erratic behavior during the RF pulse, probably due to edge heating associated with electrostatic coupling to the antenna. The temperature traces at the radial positions R ≈ 0.71, 0.66, and 0.65 m, which are shown with somewhat heavier lines, clearly indicate a temperature rise during the RF pulse. The time trace for R ≈ 0.64 m (dotted line) shows that the emission is locally cut off close to the plasma center, what gives an estimate of the central density reached during the RF pulse, i.e., $n_0 \approx 2.2 \times 10^{19}$ m^{-3}. Finally, the central chord R ≈ 0.63 m shows no temperature variation. The density due to impurity inflow [6], is rather small at the beginning of the RF pulse, as indicated by the cutoff at R = 0.64 m. However, it increases towards the end of the pulse, giving another cutoff at R = 0.71 m.

These results show that there is a localized increase of the electron temperature, which can be attributed only to direct wave absorption, in spite of the density increase. In fact, results of numerical simulations using a MHD cylindrical code indicate that the M = -1, N = -2 is preferentially excited under the conditions of this experiment. As the coupled power is rather small, P ≈ 40 kW, these experiments confirm theoretical models on localized profile modification by Alfvén waves, in advanced confinement scenarios [7].

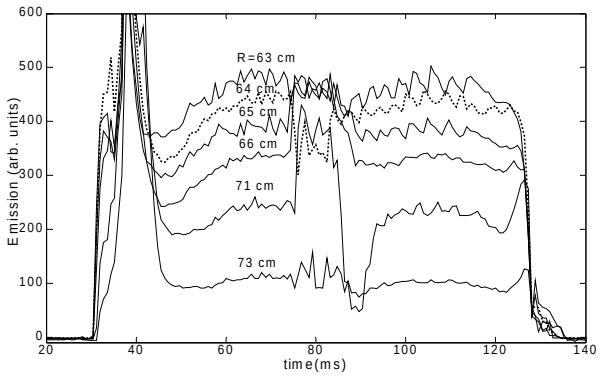

Fig. 4. Time traces of the electron temperature at different radial chords for discharge 8545. The RF pulse 80 kW, 4 MHz) is applied in the time interval 75 < t < 85 ms. The line average density at the plasma center is 1.2 × 10^{19} m^{-3} and the density profile is parabolic raised to power $\alpha \approx 0.83$.

4. RUNAWAY DISCHARGES

New experimental data on the new regime of runaway discharges found in TCABR tokamak have been obtained. The main features of this regime, which have already been presented in previous publications [4,8], are (i) relaxation instability with strong spikes of H_α emission and plasma density, (ii) plasma detachment from the limiter, and (iii) dominating role of the runaway avalanche mechanism on runaway generation. Each cycle of the relaxation instability includes a short, ~ 10 μs, pulse of beam-plasma instability followed by a stable relaxation phase with duration of 1-10 ms. In the instability phase, the plasma electron temperature increases up to T_e ~ 10 eV, resulting in an increase of plasma density due to neutral gas ionization. In the relaxation phase, the plasma temperature drops to a value around 1 eV. The main process for plasma generation and heating is collisions of runaway electrons with neutrals and thermal electrons. The plasma losses are mainly due to recombination and thermal losses by electron-ion and ion-neutral collisions. The phenomenon of plasma detachment from the limiter is caused by volume recombination. A comparison with the existing theory shows that the primary Dreicer mechanism of runaway generation is strongly suppressed, due to the low plasma temperature, except in the initial ionization phase. The secondary avalanche process can be responsible for the runaway current rise at the start-up and its maintenance in the stationary phase of the discharge [8].

One of the main questions regarding runaway discharges in tokamaks is how cold the background plasma can be [9,10]. According to our preliminary analysis, the plasma temperature in the new regime has to be rather low, to explain the observed density spikes associated with spikes in the H_α emission, and volume recombination has to be playing an important role, to justify the observed plasma detachment from the limiter due [11]. Such low temperature plasma should be almost completely transparent to neutrals and, if the model is

correct, the density and H_α spikes should be observed in the entire plasma column. This experimental evidence, which was lacking in our previous works, has been recently obtained and is presented in the sequel.

The time traces of the total plasma current, I_t , energy of the runaway electrons, W_b, H_α emission, electron density, n_e, neutral density, N_m, and electron density in the scrape-off layer, n_{sol}, are shown in Fig. 5 for two runaway discharges with different rates of neutral gas injection, higher in discharge 6693 than in 6606. We can

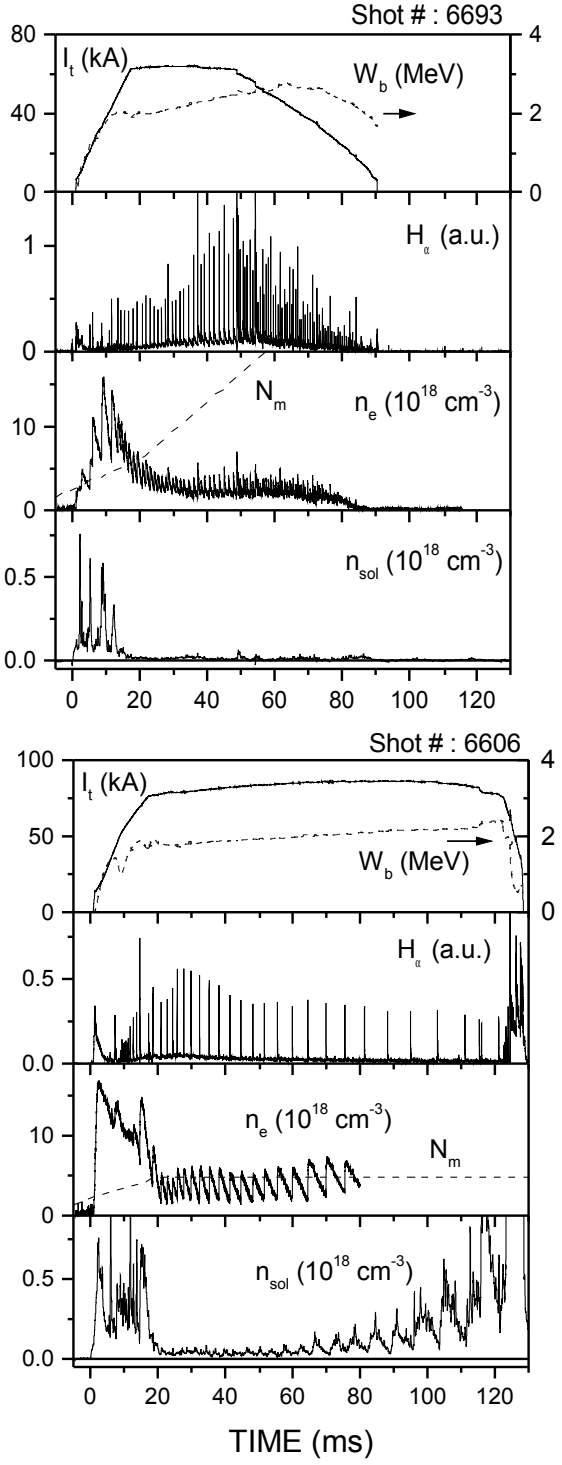

Fig. 5. Time traces of the total plasma current, I_t, H_α emission, electron density, n_e, neutral density, N_m, and electron density in the scrape-off layer, n_{sol}, for two runaway discharges with different rates of neutral gas injection, higher in discharge 6693 than in 6606.

clearly see that the frequency of the H_α and density spikes increase with the neutral gas density. Furthermore, in the low neutral density case (6606), the plasma is not completely detached from the limiter and a substantial plasma density can be measured in the scrape-off layer. The density spikes in this region are correlated with the one observed in the central chord of the interferometer but somewhat delayed and smoothed out, giving an indirect indication that the density increase in a spike occurs first in the central region of the plasma column and then diffuses out to the plasma periphery. In discharge 6693, the line average density measured in the central chord of the interferometer has approximately the same value as in discharge 6606; however, the plasma column becomes completely detached from the limiter, as can be seen from the density measured in the scrape-off layer. At $t \approx 52$ ms the plasma current starts to drop due to quenching of the discharge by the large amount of neutral gas.

According to our model, these features of the runaway discharges observed in TCABR can be explained by assuming a low - temperature background plasma kept in equilibrium by the relativistic beam current. A relaxation kinetic beam-instability is periodically triggered as the plasma density reaches a minimum threshold value, damping energy in the background plasma. As a result, the perpendicular plasma temperature increases substantially, causing a rapid increase in the ionization rate. Three questions remain to validate this model: i) which is the instability?; ii) do the ionization spikes occur in the whole plasma volume?; iii) how low is the temperature in the bulk plasma?. In the following we will address the two latter questions. To answer the first one, we still need to develop appropriate diagnostics.

5. DENSITY AND H_α PROFILES IN RUNAWAY DISCHARGES

The density measurements were performed along seven vertical chords by a two-channel microwave interferometer. Because only two chords can be used simultaneously, the density profile was determined on a shot-by-shot basis. One chord was maintained fixed at minor radius $r \approx 4$ cm in all shots, to control reproducibility of measurements. A minimum of three similar discharges is used for each point. An example of measured line densities is given in Fig. 6. The innermost radial position where the line average density can be measured is at $r \approx 17$ cm and the outmost at $r \approx 14.5$ cm, with respect to the geometric center of the plasma column ($R = 0.61$ m). As can be seen from the measurements in the control chord, the reproducibility of the discharges is quite reasonable.

The H_α emission profiles were directly measured using an array of fourteen photodiodes with optical filters viewing the plasma along vertical chords. The intensities measured by the different photodiodes were relatively calibrated using a standard lamp. The measured profiles are shown in Fig. 7 together with the pressure profile P/P_0, obtained from the equilibrium code, assuming isotropic pressure with the value of poloidal beta given by the relativistic beam energy. The profile of the H_α emission is shown in terms of its intensity at a spike, I_S,

for high and low neutral gas densities. Its relative

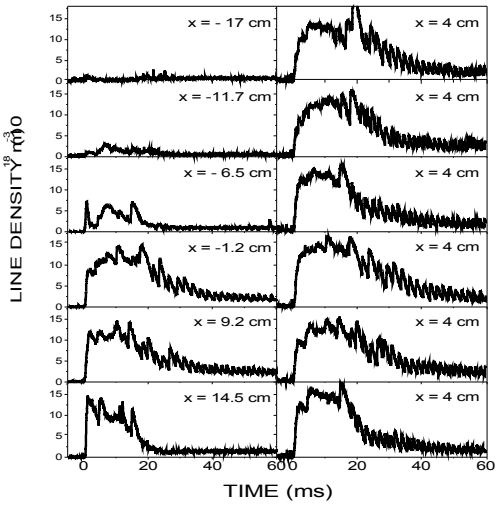

Figure 6. Line density measurements carried out on a shot-by-shot basis to determine the density profiles in runaway discharges. The channel at r ≈ 4 cm is kept fixed, to control reproducibility of the measurements, while the radial position of the other chord is varied.

amplitude can be inferred from the ratio I_R /I_S, where I_R is the emission intensity when the spike has relaxed its minimum value before the next one. The H_α emission and density profiles agree quite well. They both present a large outward shift, about 4 to 5 cm from the geometric

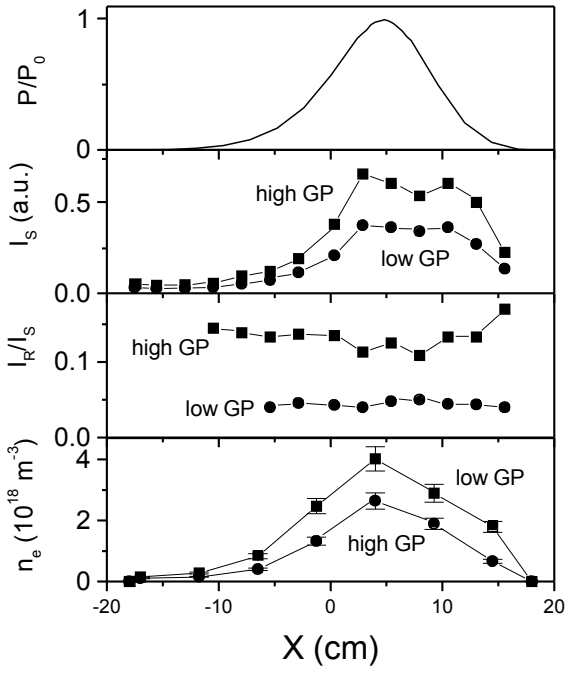

Figure 7. Radial profiles of normalized plasma pressure obtained from the equilibrium code, emission intensity at the peak of an $H_\alpha$spike, ratio of the emission intensities at the bottom and peak of the spike, and line average density for runaway discharges with low and high gas puffing rate.

axis of the last closed magnetic surface, which coincides with the limiter at r = 18 cm, within a radial accuracy of less than 1 cm, determined by feedback control of the plasma position [12]. This shift is consistent with the magnetic equilibrium predicted for relativistic electron beams with $\gamma \geq 4$ [4]. Furthermore, the broad profile of H_α emission intensity shows that ionization and recombination occur in the bulk plasma, indicating that its temperature is indeed quite low.

Unfortunately, because of the low plasma density and temperature and mode overlap due to the relativistic beam, the ECE diagnostics cannot be used even for relative measurements and, therefore, direct temperature measurement in these conditions is not a simple task. To overcome this difficulty, we have developed some indirect schemes to estimate the plasma temperature, as the one based upon the decay of loop voltage spikes [13].

Other estimates can be obtained from the rate of density increase, associated with an H_α spike, and the ratio I_R /I_S. Since the density increases quite rapidly in a spike, the ionization rate constant K_p is directly related to the rate of density rise through the expression

$$K_p(T_e, n_e) = \frac{1}{n_e N_m}\left(\frac{dn_e}{dt}\right)_S , \qquad (1)$$

where T_e and n_e are the electron and temperature density, respectively, and N_m is the neutral density. For most of the runaway discharges, we obtain $K_p \approx (0.5\text{-}1.0)\times10^{-14}$ m^{3}s^{-1}, which corresponds to $T_e \approx$ 10-15 eV at a spike.

The electron temperature at the end of a H_α spike can be estimated from the ratio I_R /I_S. Neglecting the contribution of runaways and of recombination to the emission, this ratio can be written as

$$\frac{I_R}{I_S} = \frac{S_R}{S_S} , \qquad (2)$$

where S_R and S_S are the rate constants after the spike has relaxed to the background level and at the spike maximum, respectively. For temperatures around 10 to 15 eV, these constants are approximately 10 % of the ionization rate constants, for the same values of the plasma parameters [14]. Using the known values of the density at the maximum and relaxed phases of the spike, we can estimate T_e at the relaxed phase from the measured value of I_R /I_S. For shot 6606, for example, we obtain $T_e \approx$ 3 eV, approximately. Therefore, the new regime of runaway discharges discovered in TCABR is in fact a rather peculiar beam-plasma system in which a quite low temperature plasma is kept in equilibrium by the current carried by the energetic relativistic beam.

6. CONCLUSIONS

The results of recent experiments on Alfvén wave heating and runaway discharges carried out in the TCABR tokamak have been described. Direct evidence of localized heating was obtained for the first time, at low input powers, in qualitative agreement with theoretical predictions on profile control by Alfvén waves [6]. The density and H_α emission profiles in the new regime of

runaway discharges were measured and confirm our preliminary model of these discharges [4,8].

ACKNOWLEDGEMENTS

This work has been supported by CNPq (National Council for Research and Development – Brazil), through the PRONEX Project, and by FAPESP (Foundation for Supporting Research of the State of São Paulo).

REFERENCES

[1] G S Amarante-Segundo, A G Elfimov, R M O Galvão, D W Ross, I C Nascimento; Phys. Plasmas 8, 210 (2001).

[2] L F Ruchko, E Ozono, R M O Galvão, I C Nascimento, F T. Degasperi, E Lerche; Fusion Eng. Design 43, 15 (1998).

[3] E A Lerche, E M Ozono, L Ruchko; R M O Galvão, A G Elfimov, V S Tsypin, E K Sanada, W P de Sá, I C Nascimento, Y Kuznetsov, A N Fagundes, A Vannucci, D O Campos, J I Elizondo, J H F Severo, E A Saettone, V Bellintani, A A Ferreira; American Institute of Physics Conference Proceedings 563, 191 (2001).

[4] R M O Galvão, Y Kuznetsov, I C Nascimento, E Sanada, D O Campos, A G Elfimov, J I Elizondo, A N Fagundes, A A Ferreira, A M M Fonseca, E A Lerche, R Lopez, L F Ruchko, E a Saettone, J H F Severo, R P da Silva, V S Tsypin, W P de Sá, R Valencia, A Vannucci; Plasma Physics and Controlled Fusion 43, 1181 (2001).

[5] K. Appert, G.A. Collins, T. Hellsten, J. Vaclavik, L. Villard; Plasma Phys. and Controlled Fusion 28,133 (1986).

[6] G.G. Borg, J.B. Lister, S.Dalla Piazza, Y. Martin; Nucl. Fusion 33, p.841 (1993).

[7] R M O Galvão; A G Elfimov.; G S Amarante-Segundo; V S Tsypin.; L Ruchko, I C Nascimento; M Tendler; "Alfvén Wave Heating, Current Drive, Plasma Flow and Improved Confinement Scenarios in Tokamaks"; Plasma Physics and Controlled Fusion 41, A487 (1999).

[8] R M O Galvão, V Bellintani Jr., R D Bengtson, A G Elfimov, J I Elizondo, A N Fagundes, A A Ferreira, A M M Fonseca, Y Kuznetsov, E A Lerche, I C Nascimento, L F Ruchko, E A Saettone, W P de Sá, E Sanada, J H F Severo, R P da Silva, V S Tsypin, O C Usuriaga, A Vannucci; Plasma Physics and Controlled Fusion 43, A299 (2001).

[9] V S Vlasenkov, V M Leonov, V G Mereshkin, V S Mukhovatov; Nucl. Fusion 13, 509 (1973).

[10] H Knoepfel, D A Spong, S J Zweben; Phys. Fluids 20 , 511 (1977).

[11] T K Soboleva, R M O Galvão, S I Krasheninnikov, Yu K Kuznetsov, I C Nascimento; Braz. Journal Phys. 32, 81 (2002).

[12] Yu K Kuznetsov, I C Nascimento, R M O Galvão, W P de Sá; Nucl. Fusion 38, 1385 (1998).

[13] I El Chamaa Neto, Yu K Kuznetsov, R M O Galvão, V S Tsypin; Physics of Plasmas 7, 2894 (2000).

[14] D E Post; Journal of Nuclear Materials 220-222, 143 (1995).